JCTC Journal of Chemical Theory and Computation

Article

pubs.acs.org/JCTC

Ab Initio QM/MM Study Shows a Highly Dissociated S_N2 Hydrolysis Mechanism for the cGMP-Specific Phosphodiesterase-5

Zhe Li, Yinuo Wu, Ling-Jun Feng, Ruibo Wu,* and Hai-Bin Luo*

School of Pharmaceutical Sciences, Sun Yat-Sen University, Guangzhou 510006, P. R. China

Supporting Information

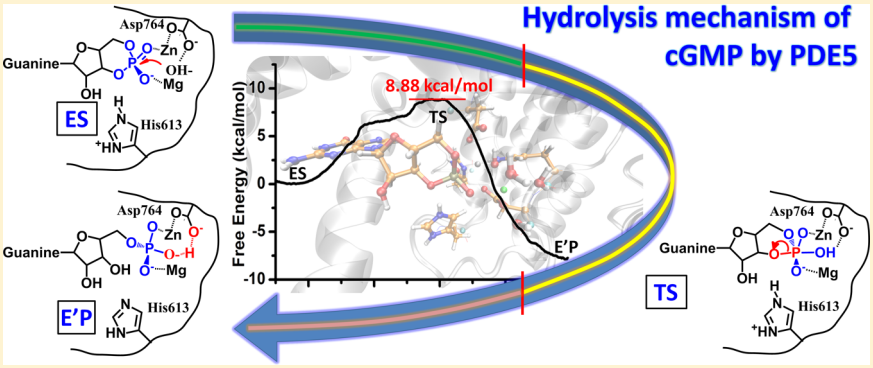

ABSTRACT: Phosphodiesterases (PDEs) are the sole enzymes hydrolyzing the important second messengers cGMP and cAMP and have been identified as therapeutic targets for several diseases. The most successful examples are PDE5 inhibitors (i.e., sildenafil and tadalafil), which have been approved for the treatment of male erectile dysfunction and pulmonary hypertension. However, the side effects mostly due to nonselective inhibition toward other PDE isoforms, set back the clinical usage of PDE5 inhibitors. Until now, the exact catalytic mechanism of the substrate cGMP by PDE5 is still unclear. Herein, the first computational study on the catalytic hydrolysis mechanism of cGMP for PDE5 (catalytic domain) is performed by employing the state-of-the-art ab initio quantum mechanics/molecular mechanics (QM/MM) molecular dynamics (MD) simulations. Our simulations show a S_N2 type reaction procedure via a highly dissociated transition state with a reaction barrier of 8.88 kcal/mol, which is quite different from the previously suggested hydrolysis mechanism of cAMP for PDE4. Furthermore, the subsequent ligand exchange and the release of the product GMP have also been investigated by binding energy analysis and MD simulations. It is deduced that ligand exchange would be the rate-determining step of the whole reaction, which is consistent with many previous experimental results. The obtained mechanistic insights should be valuable for not only the rational design of more specific inhibitors toward PDE5 but also understanding the general hydrolysis mechanism of cGMP-specific PDEs.

1. INTRODUCTION

cGMP and cAMP are the imporatnt intracellular second messengers involved in many physiological processes, such as cell growth, differentiation, exocytosis, vision, and muscle contraction.[1−7] The two messengers are synthesized by receptor-linked enzymes (e.g., adenylate cyclase and guanylate cyclase) and hydrolyzed by phosphodiesterases (PDEs), which consist of 11 families of enzymes (PDE1−11). As shown in Figure 1, PDE5, 6, and 9 are cGMP-specific enzymes and PDE4, 7, and 8 are cAMP-specific enzymes, while other PDEs (1, 2, 3, 10, and 11) can hydrolyze both cGMP and cAMP. Recently, PDEs have served as very attractive clinical targets for a range of biological disorders such as retinal degeneration, congestive heart failure, depression, asthma, erectile dysfunction, and inflammation.[8,9] The most successful examples of this drug class are PDE5 inhibitors such as sildenafil, vardenafil, tadalafil, avanafil, udenafil (Korean only), and mirodenafil (Korean only) approved for the treatment of male erectile dysfunction or pulmonary arterial hypertension.[10−13] However, since the catalytic site of the PDE isoforms are highly conserved, many side effects have been observed in PDE inhibitors due to the nonselective inhibition toward other families of PDEs, such as the visual disorders effects of PDE5 inhibitor sildenafil,[10,11] nausea and headache effects of PDE4 inhibitor roflumilast,[14] etc. Therefore, the illustration of the catalytic mechanism of cGMP/cAMP for PDEs is not only of great fundamental interest but also of high medical importance, since it would facilitate the development of more selective PDE inhibitors.

Based on the crystal structures of PDE families, each PDE contains two divalent metal ions (ME1 and ME2) in their active sites. ME1 was believed to be Zn^{2+} according to anomalous X-ray diffraction behavior and other biochemical evidence. While the second metal ion, ME2, which could not be determined according to the existing experimental results, was treated as Mg^{2+} in most studies.[15−20] The bridging ligand between the two

Received: June 13, 2014

   dx.doi.org/10.1021/ct500761d | J. Chem. Theory Comput. XXXX, XXX, XXX−XXX

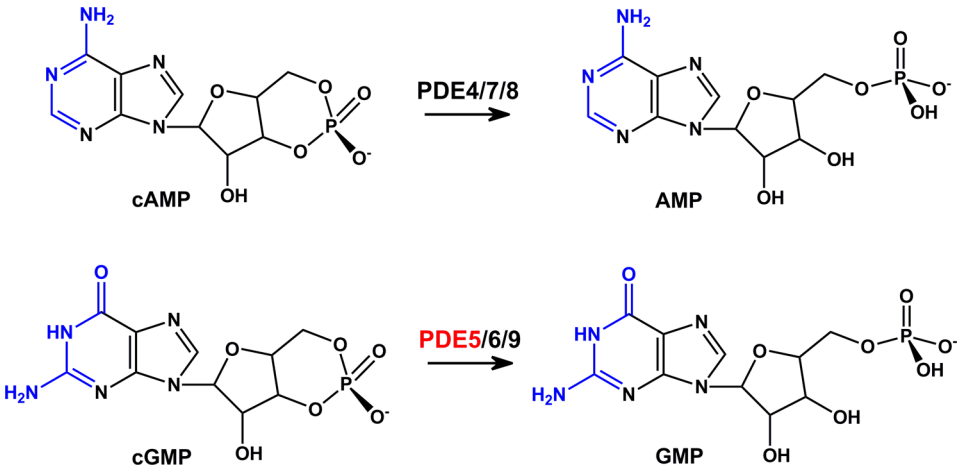

Figure 1. Specific hydrolysis of cAMP or cGMP by different PDEs. The differences between cAMP and cGMP are colored in blue, and in the present study, we focused on the hydrolysis mechanism of PDE5 toward cGMP.

metal ions was proved to be OH^- by extensive QM/MM studies.[21−23] Based on the crystal structures, three quite different catalytic mechanisms had been reported for the cAMP-specific PDE4[24−26] by employing different combined quantum mechanism/molecular mechanism (QM/MM) protocols, that is, ONIOM(B3LYP/6-31g(d):PM3) geometry optimization,[24] QM/MM (AM1:d-PhoT) molecular dynamics (MD) simulations,[26] and QM/MM (B3LYP/6-31+G(d):AMBER) free energy perturbation.[25] However, for PDE5, the only existing computational study for the catalytic mechanism of cGMP is performed on a simplified gas phase model (only five amino acids of the catalytic site) at the B3LYP/6-31G** level.[27] Until now, the exact catalytic mechanism of the cGMP-specific PDE5 is still unclear.

Herein, the computationally more expensive Born−Oppenheimer ab initio QM(DFT)/MM MD simulations were carried out to clarify the hydrolysis mechanism of cGMP catalyzed by PDE5. Taking both the fluctuation of the protein and first-principle description of the dynamics of the metal site into consideration, this method has been proved to be a state-of-the-art tool in studying the catalytic reactions in metalloenzymes.[28−34] Our result indicated that the hydrolysis stage (from ES to E′P) of the reaction follows a S_N2 type mechanism and only one transition state is involved in the initial hydrolysis procedure, which quite differs from the above-mentioned hydrolysis mechanisms for PDE4[24−26] and PDE5.[27] Moreover, the further "ligand exchange" and "product release" steps after the hydrolysis reaction were also studied. Since the computational reaction energy barriers of both the "hydrolysis stage" and the product release step are much lower than the experimental value, "ligand exchange" was deduced to be the rate-determining step of the whole enzymatic catalysis procedure. Considering the similarity of the catalytic sites between all PDEs, this S_N2 type hydrolysis mechanism by PDE5 would be very helpful for understanding the catalytic mechanisms of cGMP in other PDEs to a certain extent, as well as for the development of novel PDE5 inhibitors with higher selectivity and stronger affinity.

2. METHODS

2.1. Preparation of the PDE5-cGMP Complex. The initial structure of the enzyme−substrate complex was constructed based on the crystal structure of the PDE5A-GMP complex (PDB ID: 1T9S).[19] The ligand GMP or the product in this crystal structure was replaced by a cGMP molecule under constraint geometry optimization at the HF/6-31G* level by using the Gaussian 03 package.[35] This initial constructed binding model of cGMP in PDE5 was similar to that in the PDE9A-cGMP complex (PDB ID: 3DYL),[36] with the guanine ring of cGMP placed in the Q pocket and the phosphate ring of cGMP placed in the M pocket. Then, this constructed PDE5A-cGMP complex was equilibrated by MD simulations with AMBER 10.0.[37] First, the partial atomic charges of cGMP were obtained at the HF/6-31G* level, and then, antechamber was used to fit the restricted electrostatic potential (RESP) and to assign GAFF force field parameters to cGMP.[38] The AMBER03 force field was applied to the protein, and the "nonbond model"[39] was employed for the two metal ions in the binding site pocket. A 10-Å truncated octahedral box of TIP3P water molecules[40] was added, and Na^+ ions were used as counterions to neutralize the system. In order to coordinate with Zn^{2+}, His617 and His653 were set as HID, while His613 was set as HIP, since it would act as a proton donor during the catalytic reaction. The protonation states of other amino acid residues in the protein were determined by propka program,[41−44] and the hydrogen bond networks were further carefully checked manually. The system was first minimized by four steps of minimizations, which contained 2500 cycles of steepest descent minimization and 2500 cycles of conjugated gradient minimization in each step. Then, the system was heated from 0 to 300 K in 50 ps by using Langevin dynamics in a NVT ensemble, followed by a 100 ps of equilibration in a NPT ensemble at a pressure of 1 atm. Finally, 8 ns production step was performed in a NPT ensemble with the pressure set to 1 atm and the temperature set to 300 K. SHAKE algorithm[45] was used to constrain all the bonds involving hydrogen atoms, and the time step was set to 2 fs. During all the MD steps, the cutoff was set to 10 Å. To avoid the poor treatment of Zn^{2+} and Mg^{2+} with the selected force field, the distances between the two metal ions and the coordinated residues were restricted by a force of 400 kcal/(mol·A^2) during the whole MD simulations.[29,32−34,46,47] The trajectories became stable after 2 ns, and the resulting snapshot was used for the subsequent QM/MM studies. The RMSD plots of the backbone and the binding pocket are shown in Supporting Information Figure S1.

2.2. Born−Oppenheimer Ab Initio QM/MM MD Simulations of the Hydrolysis reaction of cGMP. The initial structure for the QM/MM MD simulations was built based

dx.doi.org/10.1021/ct500761d | J. Chem. Theory Comput. XXXX, XXX, XXX−XXX

on the snapshot after 4 ns classical MD simulations. All the solvent molecules beyond 30 Å of the zinc ion were removed to yield a spherical model containing 12,457 atoms. In this system, cGMP, His613, Asp764, Zn^{2+}, Mg^{2+}, and the coordinated OH^- were partitioned to the QM subsystem (containing 93 atoms) and other atoms were partitioned to the MM subsystem, as illustrated in Figure 2. The QM subsystem was treated by the

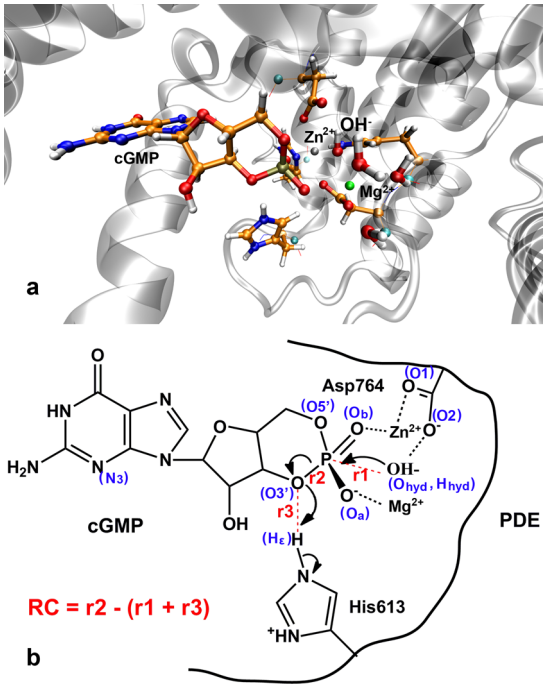

Figure 2. (a) Partition of QM and MM region. The QM region was denoted by ball and stick models. (b) The proposed hydrolysis process of cGMP catalyzed by PDEs and the reaction coordinate choice.

B3LYP method with Stuttgart ECP/basis set (SDD)[48] for the zinc ion and 6-31G* basis set for all other QM atoms. This treatment of QM regions of zinc enzymes was proved to be appropriate by many studies.[28,29,31−34] The QM/MM boundary was treated by the pseudobond approach,[49−52] while all other atoms were treated with the Amber99SB force field (comparisons between two force fields Amber99SB/ff99SB and Amber03/ff03 for the current system are given in Supporting Information).[53] Atoms more than 25 Å away from the center of the sphere were fixed. The 18- and 12-Å cutoffs were employed for electrostatic and van der Waals interactions, respectively. There was no cutoff for electrostatic interactions between QM and MM regions.

This prepared system was first optimized and followed by ∼5 ps QM/MM MD simulations, and then, QM/MM optimizations were carried out to map out a minimum energy path with the reaction coordinate deriving method.[51] As shown in Figure 2b, the distance between O_{hyd} and P was denoted by r1; the distance between P and O3′ was denoted by r2; and the distance between O3′ and H_ε was denoted by r3, respectively. There are only several possible ways to select the reaction coordinate. Four possible reaction coordinates, including -r1, r2, r2-r1, and r2-(r1+r3), were tried in this study to find the most suitable reaction coordinate. Based on these reaction coordinates, minimum energy paths were mapped out. As shown in Supporting Information Figure S2, the choices of -r1 and r2 led to wired energy curves, indicating such reaction coordinates are not acceptable for this study. The result of r2-r1 was better than that of -r1 or r2, but there still existed great energy jumps in the energy curve. The structures near the energy jumps shows that a hydrogen atom could spontaneously be transferred from His613 to O3′ (the distance between H and O is r3). Finally, r2-(r1+r3) was selected as the reaction coordinate. The forward energy curve and backward energy curve are rather smooth and are very similar (Supporting Information Figure S2), indicating this reaction coordinate is suitable for this study.

The MM subsystems for each window along the reaction coordinate were further equilibrated by 500 ps free energy perturbation calculations with the QM subsystems frozen. Based on the resulting structures, 25 ps ab initio QM/MM MD simulations with umbrella sampling were performed for each reaction window (25 windows in total) with setting 1 fs as the time-step. The harmonic biasing potentials were applied with force constants of 40 to 80 kcal/(mol·A^2). The Beeman algorithm[54] was used to integrate the Newton equation of motion, and the Berendsen thermostat method[55] was employed to control the system temperature at 300 K. The configurations from the last 20 ps trajectories of each window were used for further analysis, and the weighted histogram analysis method (WHAM)[56,57] was used to map out the unbiased potential of mean force (PMF) based on the probability distribution along the reaction coordinate. All the ab initio QM/MM calculations were performed with the modified Q-Chem[58] and Tinker[59] programs.[60]

2.3. Classical MD Simulations of the GMP Release. Following the hydrolysis stage was the dissociation between the product GMP and PDE5. The whole dissociation processes of the product GMP include ligand exchange and GMP release. After the hydrolysis stage, the two metal ions are coordinated by three oxygen atoms of the product GMP. Before the product release from the binding pocket, the three coordinating oxygen atoms would be replaced by three water molecules, which we call "ligand exchange". To study the GMP release after the hydrolysis and ligand exchange of cGMP in PDE5, the above-mentioned QM/MM reaction coordinate scanning method was employed to push the chelated product GMP away from the two metal ions. After the oxygen atoms of GMP no longer bound metal ions (at least 4 Å away from the two metal ions), the whole spherical model was transferred to be a truncated octahedral water box of 11 Å by adding many waters beyond the 30 Å spherical boundary, and further equilibrated by classical MD simulations under periodic boundary conditions for 8 ns with AMBER 10.0, with the distances between the oxygen atoms and metal ions restricted by a force of 400 kcal/(mol·A^2). Then, three water molecules occupied the former positions of the phosphate group and formed new coordinate bonds with Zn^{2+} and Mg^{2+} very fast (less than 50 ps) during MD simulations, and this resulting equilibrium structure was used to study the release procedure of the product GMP from the binding site pocket to solvent. The whole release process was also probed by the umbrella sampling based on classical MD simulations with setting distance between C-α of Ala767 and N_3 of GMP as the reaction coordinate. The whole simulations contain 50 windows with an interval of 0.2 Å, and the force constants of the harmonic biasing potentials were in a range of 30 to 60 kcal/(mol·A^2). Then, 8 ns MD simulations were performed for each window and were stable after 4 ns in all windows. Finally, the free energy profile of this product release process was yielded by using the WHAM analysis based on the stable trajectories.

dx.doi.org/10.1021/ct500761d | J. Chem. Theory Comput. XXXX, XXX, XXX−XXX

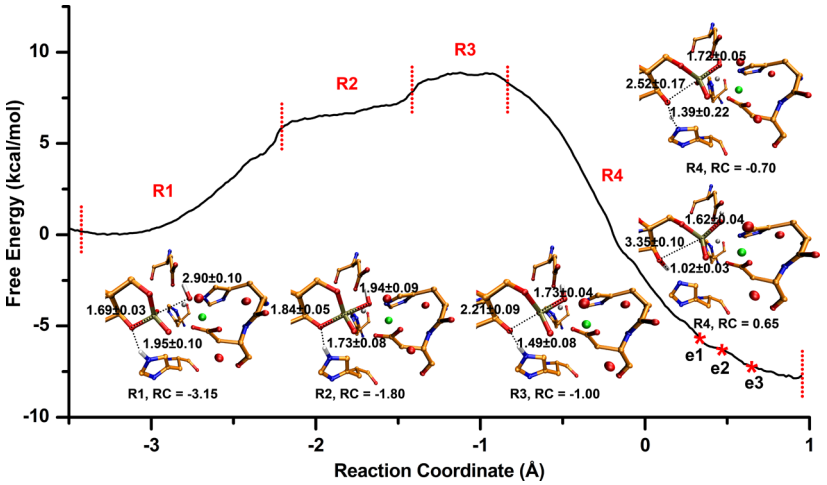

Figure 3. Potential of mean force (PMF) for the catalytic hydrolysis reaction in PDE5 along the selected reaction coordinate. R1, R2, R3, and R4 represent the 4 substages. The QM structures selected for each substage are shown as ball and stick models. e1, e2, and e3 refer to the reaction coordinates of 0.30, 0.45, and 0.65 Å, respectively.

2.4. Binding Energy Analysis of the Metal−GMP Interactions. So far, it is still not sure whether the second metal ion (ME2) is Mn^{2+} or Mg^{2+} in PDEs.[20,25,26,61] Accurately predicting the reaction barrier of the ligand exchange for the GMP-metal coordination shell is still challenging for current computational protocols. Thus, the binding energies of GMP with different metal ions were analyzed to elucidate the ligand exchange indirectly and qualitatively. Before binding energy calculations, 15 ps QM/MM MD simulations were first performed for each system. Considering that Mn^{2+} has diverse spin multiplicities, all the three possible models with different multiplicities (2, 4, and 6) were simulated. The basis set for Mn^{2+} was selected as lanl2dz, which was proved reasonable.[62] By analyzing the lowest averaged energies of the systems with the three multiplicities during the last 5 ps QM/MM MD trajectories, the most possible multiplicity is identified to be 6, which is also consistent with other metalloenzymes containing Mn^{2+} ions.[63] Then, 50 snapshots were averagely extracted from the last 5 ps trajectories to analyze the averaged binding energies. For the analysis of the binding energy, pure QM calculations by using B3LYP and the same basis set as the QM/MM MD simulations were performed on the 50 models including only GMP (set as A) as well as the two metal ions and the coordinated amino acid residues (His617, His653, Asp654, Asp764, OH^-, and three water molecules coordinating with ME2, set as B). Considering the basis set superposition error (BSSE) corrections based on the Boys−Bernardi scheme,[64,65] the corrected interaction energy E_{inter} could be calculated by using the following equations:

$$\Delta E = E_{AB}(AB) - E_A(A) - E_B(B) \quad (1)$$

$$E_{inter} = \Delta E + E_{BSSE} = E_{AB}(AB) - E_A(A) - E_B(B) + E_{BSSE} \quad (2)$$

$$E_{BSSE} = E_A(A) - E_A(AB) + E_B(B) - E_B(AB) \quad (3)$$

$$E_{inter} = E_{AB}(AB) - E_A(AB) - E_B(AB) \quad (4)$$

where $E_A(A)$ and $E_A(AB)$ represent the A subsystem calculated under the basis set of A and AB, respectively.

3. RESULTS AND DISCUSSION

3.1. Highly Dissociated S_N2 Hydrolysis Mechanism of cGMP. The PMF and representative structures of the hydrolysis reaction of cGMP catalyzed by PDE5 are shown in Figure 3. It shows a very facile concerted catalytic procedure involving only one transition state with a reaction barrier of 8.88 kcal/mol. To understand the detailed reaction process, the whole reaction is divided into 4 substages, noted as R1, R2, R3, and R4 substage, respectively. The evolution of the selected atomic distances and the charge distributions on the selected atoms are shown in Figures 4 and 5 (the values are the averaged values in each window).

At the R1 substage, the coordinated hydroxide ion (OH^-) acted as the nucleophile to attack the positive phosphate; thus, the reaction free energy profile increased steadily as the distance r1 (between O_{hyd} and phosphate atom) decreased from 2.97 to 2.35 Å. Meanwhile, the hydrogen bond between His613 and cGMP would stabilize the PDE5-cGMP complex with r3 decreasing from 2.04 to 1.73 Å. The P−O3′ ester bond was still very stable with the tiny distance change (r2 increased from 1.68 to 1.77 Å). And the coordination shell was also stable with slight distance change between Zn^{2+} and Mg^{2+}.

At the R2 substage, the reaction free energy curve was flat (Figure 3). The distance between Zn^{2+} and Mg^{2+} increased gradually due to the increase of the positive charge on the zinc ion as well as the repulsive energy between Zn^{2+} and Mg^{2+}. The negative charge on O_{hyd} began to transfer to phosphate as the O_{hyd}-P distance became shorter to almost forming chemical bond (r1 is 1.82 Å at the end of R2 substage, as shown in Figures 4 and 5). Similar to the R1 substage, the hydrogen bond between His613 and cGMP would continue to stabilize the cGMP O3′ with r3 decreasing from 1.73 to 1.59 Å. Meanwhile, due to the formation of the O_{hyd}-P covalent bond, the P−O3′ ester bond was weakened significantly with the distance r2 elongating from 1.76 to 1.94 Å, yielding a trigonal bipyramidal complex for the phosphate.

At the R3 substage, the highly dissociated transition state was maintained with the P−O3′ bond breaking from 1.94 to 2.41 Å and P−O_{hyd} bond keeping around 1.77 Å. Due to the breakage of the P−O3′ bond, more negative charge on the O3′ atom was observed. Meanwhile, the distance between Zn^{2+} and Mg^{2+} rapidly increased to about 4.3 Å and then became stable, which

dx.doi.org/10.1021/ct500761d | J. Chem. Theory Comput. XXXX, XXX, XXX−XXX

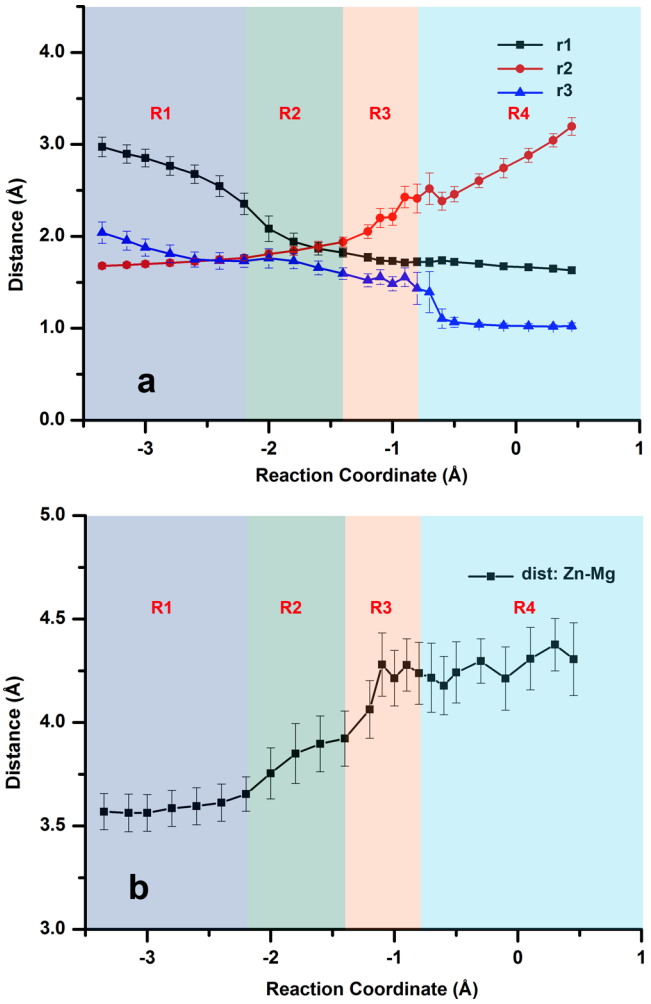

Figure 4. Evolution of the selected important distances along the hydrolysis reaction. r1, r2, and r3 correspond to the distances denoted in Figure 2b, and R1 to R4 represent the four substages of the reaction corresponding to those in Figure 3.

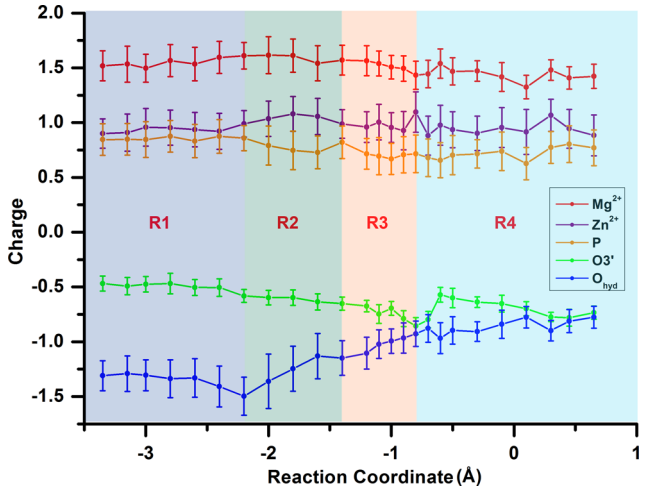

Figure 5. ESP charge distribution of Mg^{2+}, Zn^{2+}, P, O3′, and O_{hyd} atoms along the hydrolysis reaction. R1 to R4 represent the four substages of the reaction corresponding to those in Figure 3.

was caused by the negative charge migration of the hydroxide ion and the decrease of the electrostatic interactions between OH^- and the two metal ions. The coordination between Zn^{2+} and OH^- became weaker during this substage, and the distance between them was elongated from 2.1 to 2.9 Å. While the coordination between Zn^{2+} and Asp654, His617, and His653 became stronger as the distances between them decreased. The interactions between QM subsystems and its environment have been calculated for the ES, TS, and E′P state, as shown in Supporting Information Figure S3. As the reaction processes, the interaction between the QM system and its environment became stronger, indicating both the TS and E′P states could be further stabilized by the protein environment. The nucleophilic-attack reaction on phosphate atom was achieved at the end of this substage.

At the R4 substage, the tremendous reaction heat was released. At the beginning of this substage, the proton spontaneously transferred from His613 to O3′ without any reaction barrier, as shown in Figure 3, 4, and 5. Thus, it brought a suddenly decrease of negative charge on O3′ atom. Regarding the posterior of this substage, the stable product GMP was finally yielded with the further increase of P−O3′ distance. Therefore, the overall hydrolysis mechanism of cGMP catalyzed by PDE5 could be illustrated in Figure 6. First two metal ions acted as an anchor to maintain cGMP by chelating with the phosphodiester group (chelation with Oa and Ob). Then, the hydroxide ion served as the nucleophile to attack the positive phosphorus atom. Finally O3′ attracted the proton from His613 to yield the final product GMP. All of these procedures could be achieved spontaneously with only one transition state and presented a highly dissociated S_N2 hydrolysis mechanism. The one-transition-state S_N2 mechanism was further secured by performing QM/MM MD simulations with the structures of the transition state. Five snapshots were extracted from the trajectories around the transition state (RC = −1.20) to perform this calculation, and all of them were directly dropped to either the reactant ES complex or the product E′P complex (2 to ES and 3 to E′P) within 1 ps. Thus, no other intermediates exist and the proposed mechanism is reasonable. Both the substrates (cAMP and cGMP) and active sites in PDE4 and PDE5 are similar, and it is essential to compare our suggested hydrolysis mechanism of cGMP by PDE5 with the previously proposed counterpart of cAMP by PDE4. Salter and Wierzbicki[24] proposed a one-transition-state mechanism of the cAMP hydrolysis in PDE4 by ONIOM calculation, while the transition state was the proton transfer from His234 to O3′ of cAMP with an energy barrier of 3.5 kcal/mol. Wong and Gao[26] supported a two-transition-states hydrolysis reaction mechanism based on QM/MM (AM1:d-PhoT) MD simulations, first of the transition state was nucleophilic attack of OH^- toward P atom with a barrier of 13.2 kcal/mol, and the second transition state was the proton transfer from His234 to O3′ of cAMP with a barrier of ∼5 kcal/mol. Chen and Zhan[25] suggested a three-transition-states reaction mechanism from the QM/MM (B3LYP/6-31+G(d):AMBER) free energy perturbation calculations, the barrier for the three steps is 6.5, 2.2, and 2.4 kcal/mol, respectively, and the observed overall reaction barrier of the whole hydrolysis is 8.4 kcal/mol (from the reactant to the second transition state). Although only one transition state existed in our concerted S_N2 type mechanism, the three-transition-states mechanism[25] is similar to ours among the three proposed mechanisms.

3.2. Important Residues Assisting the Hydrolysis Reaction. During the reaction, the charge distributions were also analyzed. As could be seen in Figure 5, there were significant charge transfer effects in the catalytic site near the two metal ions.

dx.doi.org/10.1021/ct500761d | J. Chem. Theory Comput. XXXX, XXX, XXX−XXX

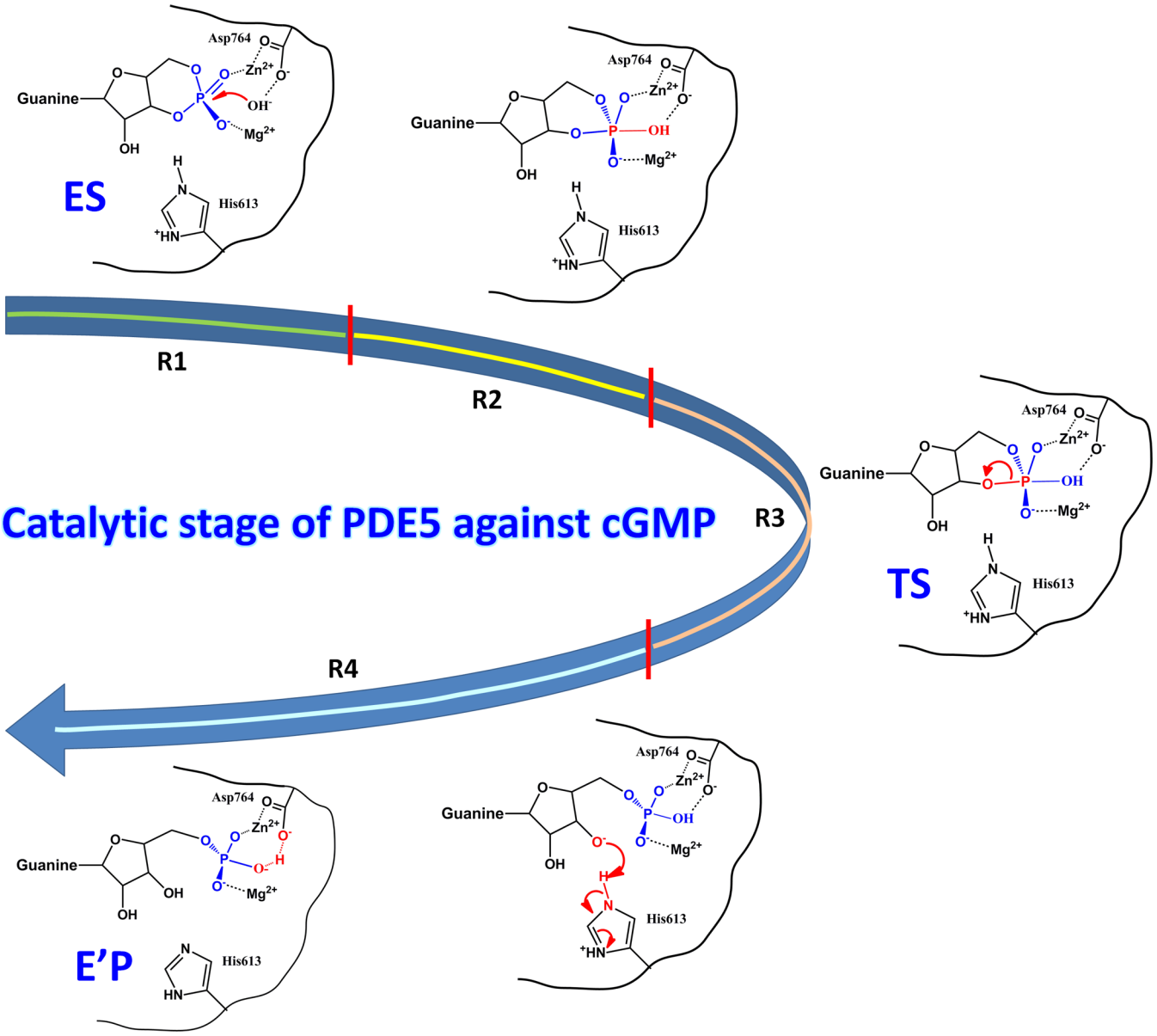

Figure 6. Proposed highly dissociated S_N2-type catalytic hydrolysis mechanism in cGMP-specific PDE5.

The charges on Mg^{2+} and Zn^{2+} were around 1.5 and 1.0, respectively; both of which were significantly lower than the formal charges of 2.0. In the catalytic site, there are many electron-rich residues assisting the hydrolysis reaction, such as His617, His653, Asp654, Asp764, and OH^-. Thus, the charge transfer from the two positive metal ions reduced the negative charges on these residues, and enhanced the stability of the catalytic site. The charges on Zn^{2+} ion were reduced much more than that on Mg^{2+} ion, which was due to two negative-charged amino acid residues (Asp654 and Asp764) coordinated with Zn^{2+} but only one (Asp654) with Mg^{2+}. Moreover, the two metal ions play as an anchor by coordinating with the phosphodiester group of cGMP during the reaction, keeping the OH^- in the right position to begin the nucleophilic attack. Thus, the two metal ions were very important for both the stability of the catalytic site and the hydrolysis reaction.

Apart from the two metal ions, the interactions between cGMP and other amino acid residues were also calculated along the reaction coordinate. The nonbond interaction energies include van der Waals interactions and electrostatic interactions, with the charges obtained from the QM/MM calculations. Residues with total energies less than −0.5 kcal/mol were plotted in Figure 7. We could see some important amino acid residues interacting with cGMP, such as Leu725, Asp764, Leu765, Val782, Phe786, and Phe820. Asp764 was located in the QM region, where as other amino acid residues were located in the MM region. These residues would make contributions to the stabilization of the transition state and could also be considered in the further inhibitor design toward PDE5.

3.3. Catalytic Roles of the Asp764-Zn Coordination Motif. At the R1 substage, Asp764 is directly coordinated to Zn^{2+} and formed hydrogen bond with OH^-. The strong hydrogen bond between Asp764 and OH^- would increase the nucleophilic capability of the O_{hyd}. As much as we know, Zn is a well lewis acid to activate the nucleophilicity of OH^- in many zinc enzymes.[23,26,66−70] Meanwhile, the zinc ion acted as an anchor to maintain cGMP and OH^- at a in-line Near-Attack-Conformation, which is thought to be very important in many

dx.doi.org/10.1021/ct500761d | J. Chem. Theory Comput. XXXX, XXX, XXX−XXX

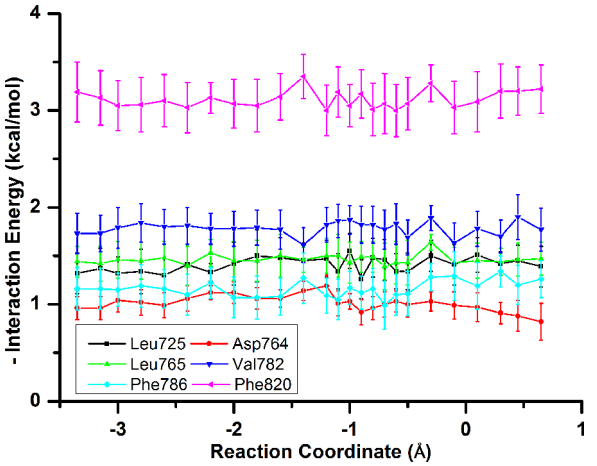

Figure 7. Energy contributions of important residues involved in the catalytic reaction. The *y*-axis is the interaction energy, and a higher value means stronger interactions.

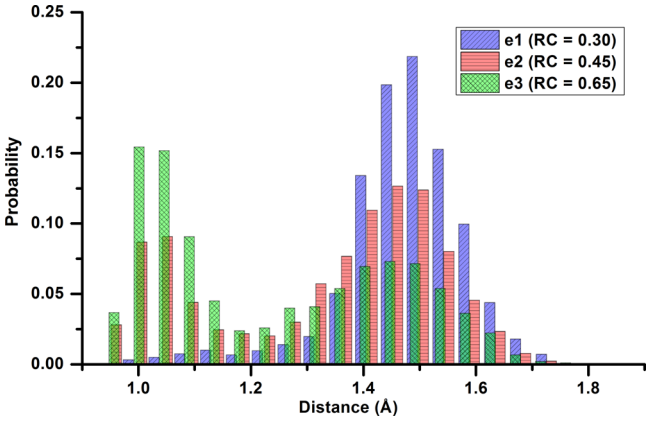

Figure 8. Probability distribution of the distance between H_{hyd} and O2 of Asp764 at three different reaction coordinates. e1, e2, and e3 refer to the reaction coordinates of 0.30, 0.45, and 0.65 Å, respectively. The H_{hyd} atom is shared by OH^- and Asp764 at the three coordinates and is more likely to appear near Asp764 as the reaction coordinate increases.

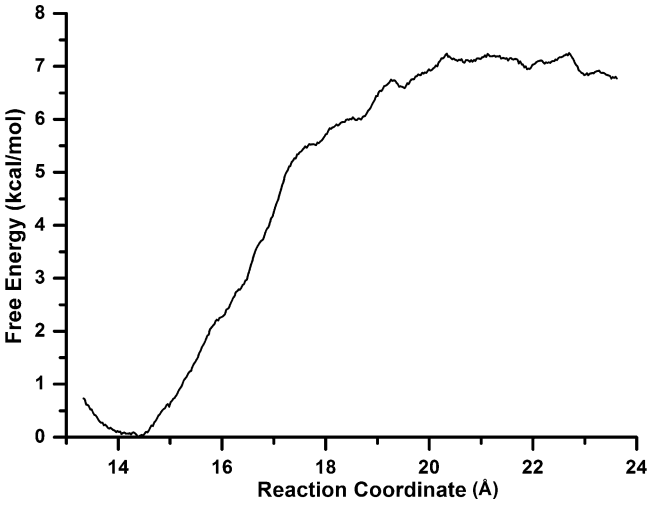

Figure 10. Potential of mean force (PMF) for the product release step. When RC = 14 Å, the product still bound the active site pocket of PDE5; when RC = 24 Å, the product was released to the surface of PDE5.

enzyme catalysis.[71,72] At the end of the R4 substage, the hydrogen atom (H_{hyd}) between OH^- and Asp764 was even shared by the two residues, as shown in Figure 8. The hydrogen atom preferred to stay on the Asp764 residue as the reaction coordinate processed to 0.65 Å, which would increase the negative charge on the O_{hyd} atom, and further stabilized the Zn^{2+} and Mg^{2+} bimetal coordination structures. As a result, it contributed to the stability of the product state.

3.4. Dissociation of the Product GMP from the Active Site Pocket of PDE5. The subsequent dissociation of the product GMP from the active site pocket could be divided into the ligand exchange and the GMP release steps, as shown in Figure 9. The energy barrier of the product release step was calculated to be about 7.23 kcal/mol as shown in Figure 10, close to the hydrolysis reaction barrier of 8.88 kcal/mol. While the observed reaction barrier should be 17.41 kcal/mol estimated from the experimental data k_{cat} of 1.3 s^{-1} for PDE5 with the transition state theory.[73] Therefore, neither the cGMP hydrolysis nor the GMP release was the rate-determining step, the ligand

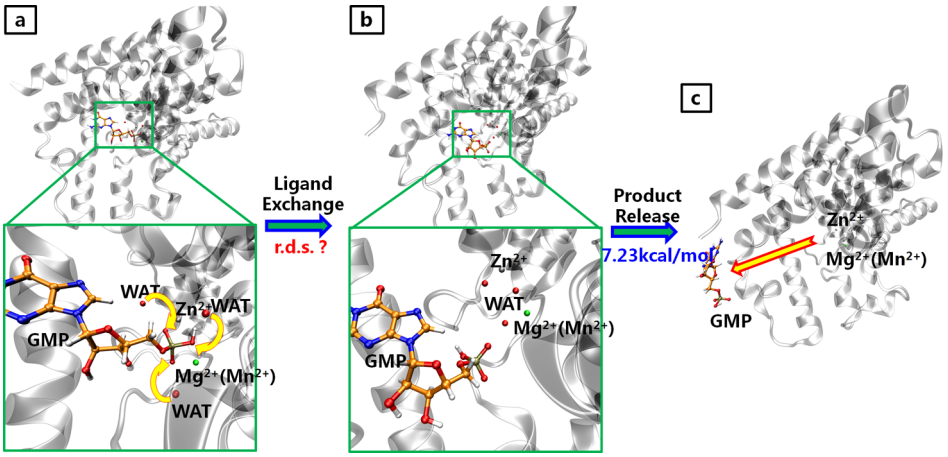

Figure 9. Dissociation of the product GMP from PDE5. This process contained a ligand exchange step and a product release step. The energy barrier of the product release step was 7.23 kcal/mol and ligand exchange was deduced to be the rate-determining step (r.d.s.). (a) Structure of the E′P complex after cGMP was hydrolyzed to GMP by PDE5. Ligand exchange (three water molecules replace three coordinating oxygen atoms of GMP) was about to happen, and yellow arrows represent one possible way of ligand exchange. (b) The binding modes of GMP in PDE5 after ligand exchange. (c) The release of GMP from the binding site pocket to the solvent.

dx.doi.org/10.1021/ct500761d | J. Chem. Theory Comput. XXXX, XXX, XXX−XXX

exchange step was very likely to be the rate-determining step of the reaction.

3.5. Catalytic Reaction in PDEs Prefers Mn^{2+} Rather than Mg^{2+} as the Catalytic Ion. Crystal structures show there are two metal ions in the catalytic site of PDEs; however, it is still not sure whether the second metal ion (ME2) is Mn^{2+} of Mg^{2+}.[15−20] If ligand exchange is the rate-determining step, the binding energy difference would directly affect the catalytic rate. Thus, the binding energy between GMP and PDE5 containing Mn^{2+} was calculated to indirectly estimate the ligand exchange difference between them. It is found that the binding between PDE5 and GMP is much stronger if ME2 is Mg^{2+}, since the averaged binding energy is 11.9 kcal/mol lower than that if Mg^{2+} is replaced by Mn^{2+}. Thus, we suggested that Mn^{2+} would be more efficient in facilitating the catalytic reaction in comparison to Mg^{2+}, which is qualitatively consistent with many experimental results. In PDE5, V_{max} is slightly higher when Mn^{2+} was used as the catalytic ion;[74] in the PDE8-cAMP system, when 4 mM $MnCl_2$ was used as the catalytic ion, the V_{max} and k_{cat} would be higher than those if using 10 mM $MgCl_2$ as the catalytic ion;[75] in PDE9, Mn^{2+} would activate the enzyme twice as much as Mg^{2+} did.[76−78] Nevertheless, more robust computational tool is required to fully understand this process in the future.

CONCLUSION

On the basis of extensive Born−Oppenheimer ab initio QM/MM MD simulations, the catalytic mechanism of PDE5 was revealed. The reaction contained two stages: the first was the hydrolysis reaction of the substrate cGMP to the product GMP and the second stage was the dissociation of GMP from PDE5. The cGMP hydrolysis was a S_N2-type reaction with a highly dissociated transition state, in which the hydroxide ion located at the middle of the two metal ions acted as the nucleophile and the reaction barrier was 8.88 kcal/mol. The Asp764-Zn coordination motif increased the nucleophilic capability of the hydroxide ion and the stability of the PDE5-GMP complex. The subsequent GMP dissociation consists of the ligand exchange and the product release steps, and the free energy barrier of the product release was about 7.23 kcal/mol. Since the energy barriers of the catalytic and the product release procedures were significantly lower than the overall observed energy barrier of the catalytic reaction determined by experiments, the ligand exchange step was deduced to be the rate-determining step of the whole catalytic reaction.

In addition, our work suggested that the catalytic reaction prefers Mn^{2+} rather than Mg^{2+} as the catalytic ion, which is also in accordance with several previous experimental results. Furthermore, according to the catalytic mechanism of PDE5, the amino acids involved in the catalytic reaction could also be considered in the further inhibitor design to improve their efficacy and specificity.

ASSOCIATED CONTENT

Supporting Information

RMSD plots of backbone and binding pocket during MM MD simulations, minimum energy path corresponding to different reaction coordinates, calculated interaction energies between QM subsystem and its environment in the ES, TS, and E′P state, comparisons between two force fields (Amber99SB/ff99SB and Amber03/ff03) for the current system. This material is available free of charge via the Internet at http://pubs.acs.org.

AUTHOR INFORMATION

Corresponding Authors

*Tel: +86-20-39943074 or +86-20-39943031. Fax: +86-20-39943000. E-mail: wurb3@mail.sysu.edu.cn.

*E-mail: luohb77@mail.sysu.edu.cn or luohb77@hotmail.com.

Notes

The authors declare no competing financial interest.

ACKNOWLEDGMENTS

We cordially thank the reviewers for the careful review and the valuable suggestions they made. This work was supported by the Natural Science Foundation of China (21103234, 21272289, and 81373258), the Guangdong Natural Science Foundation (S2011030003190 and S2013010014867), the Guangdong Science Foundation (2012A080201007), and Research Fund for the Doctoral Program of Higher Education of China (20130171110096).

REFERENCES

(1) O'Neill, J. S.; Maywood, E. S.; Chesham, J. E.; Takahashi, J. S.; Hastings, M. H. cAMP-dependent signaling as a core component of the mammalian circadian pacemaker. *Science* **2008**, *320* (5878), 949.

(2) Horvath, A.; Stratakis, C. A. Unraveling the molecular basis of micronodular adrenal hyperplasia. *Curr. Opin. Endocrinol., Diabetes Obes.* **2008**, *15* (3), 227.

(3) Hannila, S. S.; Filbin, M. T. The role of cyclic AMP signaling in promoting axonal regeneration after spinal cord injury. *Exp. Neurol.* **2008**, *209* (2), 321.

(4) Zaccolo, M.; Movsesian, M. A. cAMP and cGMP signaling cross-talk: Role of phosphodiesterases and implications for cardiac pathophysiology. *Circ. Res.* **2007**, *100* (11), 1569.

(5) Piper, M.; van Horck, F.; Holt, C. The role of cyclic nucleotides in axon guidance. *Adv. Exp. Med. Biol.* **2007**, *621*, 134.

(6) Antoni, F. A. Molecular diversity of cyclic AMP signalling. *Front. Neuroendocrinol.* **2000**, *21* (2), 103.

(7) Houslay, M. D. Adaptation in cyclic AMP signalling processes: A central role for cyclic AMP phosphodiesterases. *Semin. Cell Dev. Biol.* **1998**, *9* (2), 161.

(8) Francis, S. H.; Blount, M. A.; Corbin, J. D. Mammalian cyclic nucleotide phosphodiesterases: Molecular mechanisms and physiological functions. *Physiol. Rev.* **2011**, *91* (2), 651.

(9) Lugnier, C. Cyclic nucleotide phosphodiesterase (PDE) superfamily: A new target for the development of specific therapeutic agents. *Pharmacol. Ther.* **2006**, *109* (3), 366.

(10) Huang, Y. Y.; Li, Z.; Cai, Y. H.; Feng, L. J.; Wu, Y.; Li, X.; Luo, H. B. The molecular basis for the selectivity of tadalafil toward phosphodiesterase 5 and 6: A modeling study. *J. Chem. Inf. Model.* **2013**, *53* (11), 3044.

(11) Shang, N. N.; Shao, Y. X.; Cai, Y. H.; Guan, M.; Huang, M.; Cui, W.; He, L.; Yu, Y. J.; Huang, L.; Li, Z.; Bu, X. Z.; Ke, H.; Luo, H. B. Discovery of 3-(4-hydroxybenzyl)-1-(thiophen-2-yl)chromeno[2,3-c]-pyrrol-9(2H)-one as a phosphodiesterase-5 inhibitor and its complex crystal structure. *Biochem. Pharmacol.* **2014**, *89* (1), 86.

(12) Kyle, J. A.; Brown, D. A.; Hill, J. K. Avanafil for erectile dysfunction. *Ann. Pharmacother.* **2013**, *47* (10), 1312.

(13) Bell, A. S.; Palmer, M. J. Novel phosphodiesterase type 5 modulators: A patent survey (2008−2010). *Expert Opin. Ther. Pat.* **2011**, *21* (10), 1631.

(14) Yan, J. H.; Gu, W. J.; Pan, L. Efficacy and safety of roflumilast in patients with stable chronic obstructive pulmonary disease: A meta-analysis. *Pulm. Pharmacol. Ther.* **2014**, *27* (1), 83.

(15) Wang, H.; Liu, Y.; Hou, J.; Zheng, M.; Robinson, H.; Ke, H. Structural insight into substrate specificity of phosphodiesterase 10. *Proc. Natl. Acad. Sci. U.S.A.* **2007**, *104* (14), 5782.

(16) Zoraghi, R.; Corbin, J. D.; Francis, S. H. Phosphodiesterase-5 Gln817 is critical for cGMP, vardenafil, or sildenafil affinity: Its

orientation impacts cGMP but not cAMP affinity. *J. Biol. Chem.* **2006**, *281* (9), 5553.
(17) Iffland, A.; Kohls, D.; Low, S.; Luan, J.; Zhang, Y.; Kothe, M.; Cao, Q.; Kamath, A. V.; Ding, Y. H.; Ellenberger, T. Structural determinants for inhibitor specificity and selectivity in PDE2A using the wheat germ in vitro translation system. *Biochemistry* **2005**, *44* (23), 8312.
(18) Scapin, G.; Patel, S. B.; Chung, C.; Varnerin, J. P.; Edmondson, S. D.; Mastracchio, A.; Parmee, E. R.; Singh, S. B.; Becker, J. W.; Van der Ploeg, L. H.; Tota, M. R. Crystal structure of human phosphodiesterase 3B: Atomic basis for substrate and inhibitor specificity. *Biochemistry* **2004**, *43* (20), 6091.
(19) Zhang, K. Y.; Card, G. L.; Suzuki, Y.; Artis, D. R.; Fong, D.; Gillette, S.; Hsieh, D.; Neiman, J.; West, B. L.; Zhang, C.; Milburn, M. V.; Kim, S. H.; Schlessinger, J.; Bollag, G. A glutamine switch mechanism for nucleotide selectivity by phosphodiesterases. *Mol. Cell* **2004**, *15* (2), 279.
(20) Xu, R. X.; Hassell, A. M.; Vanderwall, D.; Lambert, M. H.; Holmes, W. D.; Luther, M. A.; Rocque, W. J.; Milburn, M. V.; Zhao, Y.; Ke, H.; Nolte, R. T. Atomic structure of PDE4: Insights into phosphodiesterase mechanism and specificity. *Science* **2000**, *288* (5472), 1822.
(21) Xiong, Y.; Lu, H. T.; Zhan, C. G. Dynamic structures of phosphodiesterase-5 active site by combined molecular dynamics simulations and hybrid quantum mechanical/molecular mechanical calculations. *J. Comput. Chem.* **2008**, *29* (8), 1259.
(22) Xiong, Y.; Lu, H. T.; Li, Y.; Yang, G. F.; Zhan, C. G. Characterization of a catalytic ligand bridging metal ions in phosphodiesterases 4 and 5 by molecular dynamics simulations and hybrid quantum mechanical/molecular mechanical calculations. *Biophys. J.* **2006**, *91* (5), 1858.
(23) Zhan, C. G.; Zheng, F. First computational evidence for a catalytic bridging hydroxide ion in a phosphodiesterase active site. *J. Am. Chem. Soc.* **2001**, *123* (12), 2835.
(24) Salter, E. A.; Wierzbicki, A. The mechanism of cyclic nucleotide hydrolysis in the phosphodiesterase catalytic site. *J. Phys. Chem. B* **2007**, *111* (17), 4547.
(25) Chen, X.; Zhao, X.; Xiong, Y.; Liu, J.; Zhan, C. G. Fundamental reaction pathway and free energy profile for hydrolysis of intracellular second messenger adenosine 3′,5′-cyclic monophosphate (cAMP) catalyzed by phosphodiesterase-4. *J. Phys. Chem. B* **2011**, *115* (42), 12208.
(26) Wong, K. Y.; Gao, J. Insight into the phosphodiesterase mechanism from combined QM/MM free energy simulations. *FEBS J.* **2011**, *278* (14), 2579.
(27) Cao, X. R.; Liu, C. B.; Liu, Y. J. Theoretical studies on the mechanism of cyclic nucleotide monophosphate hydrolysis within phosphodiesterases. *J. Theor. Comput. Chem.* **2012**, *11* (3), 573.
(28) Corminboeuf, C.; Hu, P.; Tuckerman, M. E.; Zhang, Y. Unexpected deacetylation mechanism suggested by a density functional theory QM/MM study of histone-deacetylase-like protein. *J. Am. Chem. Soc.* **2006**, *128* (14), 4530.
(29) Wu, R.; Hu, P.; Wang, S.; Cao, Z.; Zhang, Y. Flexibility of catalytic zinc coordination in thermolysin and HDAC8: A Born−Oppenheimer ab initio QM/MM molecular dynamics study. *J. Chem. Theory Comput.* **2009**, *6* (1), 337.
(30) Sousa, S. F.; Fernandes, P. A.; Ramos, M. J. The carboxylate shift in zinc enzymes: A computational study. *J. Am. Chem. Soc.* **2007**, *129* (5), 1378.
(31) Xiao, C.; Zhang, Y. Catalytic mechanism and metal specificity of bacterial peptide deformylase: A density functional theory QM/MM study. *J. Phys. Chem. B* **2007**, *111* (22), 6229.
(32) Wu, R.; Lu, Z.; Cao, Z.; Zhang, Y. Zinc chelation with hydroxamate in histone deacetylases modulated by water access to the linker binding channel. *J. Am. Chem. Soc.* **2011**, *133* (16), 6110.
(33) Wu, R.; Xie, H.; Cao, Z.; Mo, Y. Combined quantum mechanics/molecular mechanics study on the reversible isomerization of glucose and fructose catalyzed by *Pyrococcus furiosus* phosphoglucose isomerase. *J. Am. Chem. Soc.* **2008**, *130* (22), 7022.
(34) Wu, R.; Gong, W.; Liu, T.; Zhang, Y.; Cao, Z. QM/MM molecular dynamics study of purine-specific nucleoside hydrolase. *J. Phys. Chem. B* **2012**, *116* (6), 1984.
(35) Frisch, M. J.; Trucks, G. W.; Schlegel, H. B.; Scuseria, G. E.; Robb, M. A.; Cheeseman, J. R.; Montgomery, J. A.; Vreven, T.; Kudin, K. N.; Burant, J. C.; Millam, J. M.; Iyengar, S. S.; Tomasi, J.; Barone, V.; Mennucci, B.; Cossi, M.; Scalmani, G.; Rega, N.; Petersson, G. A.; Nakatsuji, H.; Hada, M.; Ehara, M.; Toyota, K.; Fukuda, R.; Hasegawa, J.; Ishida, M.; Nakajima, T.; Honda, Y.; Kitao, O.; Nakai, O.; Klene, M.; Li, X.; Knox, J. E.; Hratchian, H. P.; Cross, J. B.; Bakken, V.; Adamo, C.; Jaramillo, J.; Gomperts, R.; Stratmann, R. E.; Yazyev, O.; Austin, A. J.; Cammi, R.; Pomelli, C.; Ochterski, J. W.; Ayala, P. Y.; Morokuma, K.; Voth, G. A.; Salvador, P.; Dannenberg, J. J.; Zakrzewski, V. G.; Dapprich, S.; Daniels, A. D.; Strain, M. C.; Farkas, O.; Malick, D. K.; Rabuck, A. D.; Raghavachari, K.; Foresman, J. B.; Ortiz, J. V.; Cui, Q.; Baboul, A. G.; Clifford, S.; Cioslowski, J.; Stefanov, B. B.; Liu, G.; Liashenko, A.; Piskorz, P.; Komaromi, I.; Martin, R. L.; Fox, D. J.; Keith, T.; Al-Laham, M. A.; Peng, C. Y.; Nanayakkara, A.; Challacombe, M.; Gill, P. M. W.; Johnson, B.; Chen, W.; Wong, M. W.; Gonzalez, C.; Pople, J. A. *Gaussian 03*, Revision E.01; Gaussian, Inc.: Pittsburgh, PA, 2004.
(36) Liu, S.; Mansour, M. N.; Dillman, K. S.; Perez, J. R.; Danley, D. E.; Aeed, P. A.; Simons, S. P.; Lemotte, P. K.; Menniti, F. S. Structural basis for the catalytic mechanism of human phosphodiesterase 9. *Proc. Natl. Acad. Sci. U.S.A.* **2008**, *105* (36), 13309.
(37) Case, D. A.; Darden, T. A.; Cheatham, T. E. I.; Simmerling, C. L.; Wang, J.; Duke, R. E.; Luo, R.; Walker, R. C.; Zhang, W.; Merz, K. M.; Roberts, B. P.; Hayik, S.; Roitberg, A.; Seabra, G.; Swails, J.; Götz, A. W.; Kolossváry, I.; Wong, K. F.; Paesani, F.; Vanicek, J.; Wolf, R. M.; Liu, J.; Wu, X.; Brozell, S. R.; Steinbrecher, T.; Gohlke, H.; Cai, Q.; Ye, X.; Wang, J.; Hsieh, M. J.; Cui, G.; Roe, D. R.; Mathews, D. H.; Seetin, M. G.; Salomon-Ferrer, R.; Sagui, C.; Babin, V.; Luchko, T.; Gusarov, S.; Kovalenko, A.; Kollman, P. A. *AMBER 10*; University of California: San Francisco, 2008.
(38) Wang, J.; Wang, W.; Kollman, P. A.; Case, D. A. Automatic atom type and bond type perception in molecular mechanical calculations. *J. Mol. Graph. Modell.* **2006**, *25* (2), 247.
(39) Stote, R. H.; Karplus, M. Zinc binding in proteins and solution: A simple but accurate nonbonded representation. *Proteins* **1995**, *23* (1), 12.
(40) Jorgensen, W.; Chandrasekhar, J.; Madura, J.; Impey, R.; Klein, M. Comparison of simple potential functions for simulating liquid water. *J. Chem. Phys.* **1983**, *79* (2), 926.
(41) Li, H.; Robertson, A. D.; Jensen, J. H. Very fast empirical prediction and rationalization of protein pK_a values. *Proteins* **2005**, *61* (4), 704.
(42) Bas, D. C.; Rogers, D. M.; Jensen, J. H. Very fast prediction and rationalization of pK_a values for protein−ligand complexes. *Proteins* **2008**, *73* (3), 765.
(43) Olsson, M.; Sondergaard, C. R.; Rostkowski, M.; Jensen, J. H. PROPKA3: Consistent treatment of internal and surface residues in empirical pK_a predictions. *J. Chem. Theory Comput.* **2011**, *7* (2), 525.
(44) Sondergaard, C. R.; Olsson, M.; Rostkowski, M.; Jensen, J. H. Improved treatment of ligands and coupling effects in empirical calculation and rationalization of pK_a values. *J. Chem. Theory Comput.* **2011**, *7* (7), 2284.
(45) Shuichi, M.; Kollman, P. A. Settle: An analytical version of the SHAKE and RATTLE algorithm for rigid water models. *J. Comput. Chem.* **1992**, *8* (13), 952.
(46) Liang, J. Y.; Lipscomb, W. N. Binding of substrate CO_2 to the active site of human carbonic anhydrase II: A molecular dynamics study. *Proc. Natl. Acad. Sci. U.S.A.* **1990**, *87* (10), 3675.
(47) Abedi, K. R.; Abdul, R. M.; Basri, M.; Salleh, A. B.; Jacobs, D.; Abdul, W. H. Molecular dynamics study of the structure, flexibility and dynamics of thermostable l1 lipase at high temperatures. *Protein J.* **2009**, *28* (1), 14.
(48) Dolg, M.; Wedig, U.; Stoll, H.; Preuss, H. Energy-adjusted abinitio pseudopotentials for the first row transition elements. *J. Chem. Phys.* **1987**, *86* (2), 866.

(49) Zhang, Y. Pseudobond ab initio QM/MM approach and its applications to enzyme reactions. *Theor. Chem. Acc.* **2006**, *116* (1−3), 43.
(50) Zhang, Y.; Lee, T. S.; Yang, W. A pseudobond approach to combining quantum mechanical and molecular mechanical methods. *J. Chem. Phys.* **1999**, *110* (1), 46.
(51) Zhang, Y.; Liu, H.; Yang, W. Free energy calculation on enzyme reactions with an efficient iterative procedure to determine minimum energy paths on a combined ab initio QM/MM potential energy surface. *J. Chem. Phys.* **2000**, *112* (8), 3483.
(52) Zhang, Y. Improved pseudobonds for combined ab initio quantum mechanical/molecular mechanical methods. *J. Chem. Phys.* **2004**, *122* (2), 24114.
(53) Cornell, W. D.; Cieplak, P.; Bayly, C. I.; Gould, I. R.; Merz, K. M.; Ferguson, D. M.; Spellmeyer, D. C.; Fox, T.; Caldwell, J. W.; Kollman, P. A. A second generation force field for the simulation of proteins, nucleic acids, and organic molecules. *J. Am. Chem. Soc.* **1995**, *117* (19), 5179.
(54) Beeman, D. Some multistep methods for use in molecular dynamics calculations. *J. Comput. Phys.* **1976**, *20* (2), 130.
(55) Berendsen, H. J.; Postma, J. P. M.; van Gunsteren, W. F.; DiNola, A. R. H. J.; Haak, J. R. Molecular dynamics with coupling to an external bath. *J. Chem. Phys.* **1984**, *81* (8), 3684.
(56) Kumar, S.; Rosenberg, J. M.; Bouzida, D.; Swendsen, R. H.; Kollman, P. A. The weighted histogram analysis method for free-energy calculations on biomolecules. I. The method. *J. Comput. Chem.* **1992**, *13* (8), 1011.
(57) Souaille, M.; Roux, B. Extension to the weighted histogram analysis method: Combining umbrella sampling with free energy calculations. *Comput. Phys. Commun.* **2001**, *135* (1), 40.
(58) Shao, Y.; Fusti-Molnar, L.; Jung, Y.; Kussmann, J.; Ochsenfeld, C.; Brown, S. T.; Gilbert, A. T. B.; Slipchenko, L. V.; Levchenko, S. V.; O'Neill, D. P.; Jr. DiStasio, R. A.; Lochan, R. C.; Wang, T.; Beran, G. J. O.; Besley, N. A.; Herbert, J. M.; Lin, C. Y.; Van Voorhis, T.; Chien, S. H.; Sodt, A.; Steele, R. P.; Rassolov, V. A.; Maslen, P. E.; Korambath, P. P.; Adamson, R. D.; Austin, B.; Baker, J.; Byrd, E. F. C.; Dachsel, H.; Doerksen, R. J.; Dreuw, A.; Dunietz, B. D.; Dutoi, A. D.; Furlani, T. R.; Gwaltney, S. R.; Heyden, A.; Hirata, S.; Hsu, C. P.; Kedziora, G.; Khaliullin, R. Z.; Klunzinger, P.; Lee, A. M.; Lee, M. S.; Liang, W.; Lotan, I.; Nair, N.; Peters, B.; Proynov, E. I.; Pieniazek, P. A.; Rhee, Y. M.; Ritchie, J.; Rosta, E.; Sherrill, C. D.; Simmonett, A. C.; Subotnik, J. E.; III, H. L. W.; Zhang, W.; Bell, A. T.; Chakraborty, A. K.; Chipman, D. M.; Keil, F. J.; Warshel, A.; Hehre, W. J.; III, H. F. S.; Kong, J.; Krylov, A. I.; Gill, P. M. W.; Head-Gordon, M.; Gan, Z.; Zhao, Y.; Schultz, N. E.; Truhlar, D.; Epifanovsky, E.; Oana, M.; Baer, R.; Brooks, B. R.; Casanova, D.; Chai, J. D.; Cheng, C. L.; Cramer, C.; Crittenden, D.; Ghysels, A.; Hawkins, G.; Hohenstein, E. G.; Kelley, C.; Kurlancheek, W.; Liotard, D.; Livshits, E.; Manohar, P.; Marenich, A.; Neuhauser, D.; Olson, R.; Rohrdanz, M. A.; Thanthiriwatte, K. S.; Thom, A. J. W.; Vanovschi, V.; Williams, C. F.; Wu, Q.; You., Z. Q.; Aspuru-Guzik, A.; Chang, C.; Edgar, R. G.; Sundstrom, E.; Parkhill, J.; Lawler, K.; Gordon, M.; Schmidt, M.; Shenvi, N.; Lambrecht, D.; Goldey, M.; Olivares-Amaya, R.; Bernard, Y.; Vogt, L.; Watson, M.; Liu, J.; Yeganeh, S.; Kaduk, B.; Vydrov, O.; Xu, X.; Kaliman, I.; Khistyaev, K.; Russ, N.; Zhang, I. Y.; III, W. A. G.; Liu, F.; King, R.; Landau, A.; Wormit, M.; Dreuw, A.; Diedenhofen, M.; Klamt, A.; Lange, A. W.; Ghosh, D.; Kosenkov, D.; Kus, T.; Landau, A.; Zuev, D.; Deng, J.; Mao, S. P.; Su, Y. C.; Small, D. *Q-Chem.*, Version 4.0; Q-Chem, Inc.: Pittsburgh, PA, 2007.
(59) Ponder, J. W. *TINKER, Software Tools for Molecular Design*, version 4.2; Washington University School of Medicine: St. Louis, MO, 2004.
(60) Wang, S. L.; Hu, P.; Zhang, Y. K. Ab initio quantum mechanical/molecular mechanical molecular dynamics simulation of enzyme catalysis: The case of histone lysine methyltransferase SET7/9. *J. Phys. Chem. B* **2007**, *111* (14), 3758.
(61) Huai, Q.; Colicelli, J.; Ke, H. The crystal structure of AMP-bound PDE4 suggests a mechanism for phosphodiesterase catalysis. *Biochemistry* **2003**, *42* (45), 13220.
(62) Nayak, S. K.; Jena, P. Equilibrium geometry, stability, and magnetic properties of small MnO clusters. *J. Am. Chem. Soc.* **1999**, *121* (4), 644.
(63) Liao, R. Z.; Thiel, W. Determinants of regioselectivity and chemoselectivity in fosfomycin resistance protein FosA from QM/MM calculations. *J. Phys. Chem. B* **2013**, *117* (5), 1326.
(64) Non-empirical molecular orbital calculations on the protonation of carbon monoxide. *Chem. Phys. Lett.* **1969**, *3* (3), 140.
(65) The calculation of small molecular interactions by the differences of separate total energies. Some procedures with reduced errors. *Mol. Phys.* **1970**, *19* (4), 553.
(66) Zhang, X.; Wu, R. B.; Song, L. C.; Lin, Y. C.; Lin, M. H.; Cao, Z. X.; Wu, W.; Mo, Y. R. Molecular dynamics simulations of the detoxification of paraoxon catalyzed by phosphotriesterase. *J. Comput. Chem.* **2009**, *30* (15), 2388.
(67) Wong, K. Y.; Gao, J. The reaction mechanism of paraoxon hydrolysis by phosphotriesterase from combined QM/MM simulations. *Biochemistry* **2007**, *46* (46), 13352.
(68) Xiong, Y.; Lu, H. T.; Li, Y. J.; Yang, G. F.; Zhan, C. G. Characterization of a catalytic ligand bridging metal ions in phosphodiesterases 4 and 5 by molecular dynamics simulations and hybrid quantum mechanical/molecular mechanical calculations. *Biophys. J.* **2006**, *91* (5), 1858.
(69) Hou, G. H.; Cui, Q. Stabilization of different types of transition states in a single enzyme active site: QM/MM analysis of enzymes in the alkaline phosphatase superfamily. *J. Am. Chem. Soc.* **2013**, *135* (28), 10457.
(70) Hou, G. H.; Cui, Q. QM/MM analysis suggests that alkaline phosphatase (AP) and nucleotide pyrophosphatase/phosphodiesterase slightly tighten the transition state for phosphate diester hydrolysis relative to solution: Implication for catalytic promiscuity in the AP superfamily. *J. Am. Chem. Soc.* **2012**, *134* (1), 229.
(71) Rodrigues, J. R.; Couto, A.; Cabezas, A.; Pinto, R. M.; Ribeiro, J. M.; Canales, J.; Costas, M. J.; Cameselle, J. C. Bifunctional homodimeric triokinase/FMN cyclase: Contribution of protein domains to the activities of the human enzyme and molecular dynamics simulation of domain movements. *J. Biol. Chem.* **2014**, *289* (15).
(72) Kotsakis, S. D.; Caselli, E.; Tzouvelekis, L. S.; Petinaki, E.; Prati, F.; Miriagou, V. Interactions of oximino-substituted boronic acids and β-lactams with the CMY-2-derived extended-spectrum cephalosporinases CMY-30 and CMY-42. *Antimicrob. Agents Ch.* **2013**, *57* (2), 968.
(73) Wang, H.; Liu, Y.; Huai, Q.; Cai, J.; Zoraghi, R.; Francis, S. H.; Corbin, J. D.; Robinson, H.; Xin, Z.; Lin, G.; Ke, H. Multiple conformations of phosphodiesterase-5: Implications for enzyme function and drug development. *J. Biol. Chem.* **2006**, *281* (30), 21469.
(74) Francis, S. H.; Turko, I. V.; Grimes, K. A.; Corbin, J. D. Histidine-607 and histidine-643 provide important interactions for metal support of catalysis in phosphodiesterase-5. *Biochemistry* **2000**, *39* (31), 9591.
(75) Yan, Z.; Wang, H.; Cai, J.; Ke, H. Refolding and kinetic characterization of the phosphodiesterase-8A catalytic domain. *Protein Expr. Purif.* **2009**, *64* (1), 82.
(76) Huai, Q.; Wang, H. C.; Zhang, W.; Colman, R. W.; Robinson, H.; Ke, H. M. Crystal structure of phosphodiesterase 9 shows orientation variation of inhibitor 3-isobutyl-1-methylxanthine binding. *Proc. Natl. Acad. Sci. U.S.A.* **2004**, *101* (26), 9624.
(77) Fisher, D. A.; Smith, J. F.; Pillar, J. S.; Denis, S. H. S.; Cheng, J. B. Isolation and characterization of PDE9A, a novel human cGMP-specific phosphodiesterase. *J. Biol. Chem.* **1998**, *273* (25), 15559.
(78) Wang, P.; Wu, P.; Egan, R. W.; Billah, M. M. Identification and characterization of a new human type 9 eGMP-specific phosphodiesterase splice variant (PDE9A5)—Differential tissue distribution and subcellular localization of PDE9A variants. *Gene* **2003**, *314*, 15.